Proceedings of the 29th Annual International
Conference of the IEEE EMBS
Cité Internationale, Lyon, France
August 23-26, 2007.

Evaluation of the Visual System in a Rat Model of Chronic Glaucoma using Manganese-enhanced Magnetic Resonance Imaging

Kevin C. Chan[1,2], Qing-ling Fu[3], Kwok-fai So[3], and Ed X. Wu[1,2]

[1] Laboratory of Biomedical Imaging and Signal Processing, [2] Department of Electrical and Electronic Engineering,
[3] Department of Anatomy, The University of Hong Kong, Pokfulam, Hong Kong
Correspondence to: Ed X. Wu, Tel: (852) 2819-9713, Fax: (852) 2819-9711, Email: ewu@eee.hku.hk

Abstract—**This study aims to employ *in vivo* manganese-enhanced MRI (MEMRI) to evaluate dynamically the Mn^{2+} enhancements along the visual pathway following an induction of ocular hypertension in a rat model of chronic glaucoma. Results showed an accumulation of Mn^{2+} ions in the vitreous humor of the glaucomatous eye, with no statistical changes in the total retinal thickness but a possible occlusion of the ions at the optic nerve head. Meanwhile, there was a reduction in Mn^{2+} transport in the glaucomatous optic nerve in the later stage of our model. Fewer enhancements in the visual cortex projected from the glaucomatous eye were also detectable. These may help understand the disease mechanisms, monitor the effect of drug interventions to glaucoma models, and complement the conventional techniques in examining the visual components.**

I. INTRODUCTION

Glaucoma is a neurodegenerative disease of the visual system characterized by retinal ganglion cell (RGC) death, optic nerve head (ONH) damage, and progressive visual field loss [1]. It is the second major cause of blindness in the world [2]. While elevated intraocular pressure (IOP) is considered to be a major risk factor, the primary cause to the disease mechanisms is still unclear [3]. Quantitative assessments of optic nerve axonal loss or brain changes in experimental models of glaucoma are typically done postmortem in histological tissue sections [4-5]. To study the exact mechanisms of glaucomatous changes, there is a need to develop a novel, *in vivo*, three-dimensional method to investigate into the integrity of the primary visual system longitudinally.

Magnetic resonance imaging (MRI) provides a non-invasive tool to study the inner-depths of the body *in vivo*. Among the MRI techniques, manganese-enhanced magnetic resonance imaging (MEMRI) has been increasingly used to study the enhancement of the cytoarchitecture, tract-tracing of the neuronal pathways and the activated regions in the brain [6]. The Mn^{2+} ions are paramagnetic in nature and can shorten the T_1 relaxation time of the surrounding water protons. They act as a calcium analogue and enter the intracellular space via L-type voltage-gated calcium channels upon neuronal activation [7]. The ions are then sequestered in the endoplasmic reticulum and actively transported along the microtubules via fast axonal transport [8, 9]. It has been suggested that glial uptake and diffusion may also contribute to the cerebral pattern in Mn^{2+} enhancement [9]. MEMRI had been used to examine the vitreous humor, retina, optic nerves (ONs), lateral geniculate nuclei (LGN), superior colliculi (SC) and the visual cortex of the rat visual system. In this study, we attempted to examine the Mn^{2+} transport in the normal and glaucomatous eyes upon intravitreal injection, to correlate the *in vivo* results with previous histological findings, and to optimize the investigation into the integrity of the visual system and the possibility of ocular drug delivery to the glaucomatous eyes.

Mn^{2+} had been applied transsclerally, transcorneally and intravitreally to evaluate its distribution in the eyeballs for ocular drug delivery [10-11]. The glaucoma model in the current study involves laser photocoagulation of the episcleral and limbal veins, which contributes to the obstruction of aqueous outflow in rats [12]. Blockade of this drainage would induce a 1.6-fold increase in IOP [13]. By employing dynamic MEMRI, we hypothesize that the usual pattern of Mn^{2+} clearance in the glaucomatous eyeball will be perturbed upon intravitreal injection.

Meanwhile, previous studies using high-resolution MEMRI detected layer-specific retinal functional adaptation [14], as well as changes in intraretinal signal intensities in a rat model of choroidal melanoma [15]. The chronic IOP elevation in our model was proven to induce a 3% RGC loss per week across the 8-week experimental period [13]; Further, it was shown that ocular hypertension might accompany with ischemia, axonal swelling and mechanical alteration of the laminar layers at the ONH [3]. To account for these, we would attempt to evaluate the signal changes in the retina and the ONH in the experimental and control eyes.

As Mn^{2+} can access the nervous system intraaxonally without the reliance on hemodynamic response, studies evaluated the axonal transport rate in Alzheimer's disease and upon drug treatment [16]; On the other hand, axon degeneration had been demonstrated by the blockade of Mn^{2+} transport at the sites of radiation-induced injury [17] and ON crush upon intravitreal injection [18]. It is also possible to compare the cross-sectional areas in the prechiasmatic regions of the ON induced with optic glioma in the same coronal slice as generally the prechiasmatic ONs are parallel to one another [19]. In the glaucoma model, reports indicated an early damage from elevated IOP in rats in the superior regions of the ON [4], whereas the axoplasmic flow might be disturbed upon chronic IOP elevation [20]. Therefore, we hypothesize that there would be a reduction in Mn^{2+} transport along the glaucomatous ON, especially in the superior regions.

Lastly, previous studies demonstrated the delineation of the rat visual cortex using MEMRI [5, 21]. Among which, enhancement of the cortical layers via intracameral injection

involved transsynaptic transport of Mn^{2+} ions from the terminals of the SC and LGN to the primary visual cortex (V1) and from V1 to the extrastriate visual cortex (V2L). In primate glaucoma, pathological examination of the LGN revealed marked degenerative changes [22]. A recent report had also provided postmortem human glaucoma evidence for neuropathology in the LGN and visual cortex in the severe case [23]. Thus, we propose that the distal components of the glaucomatous rat visual pathway may be vulnerable to signal reduction as shown by MEMRI, especially in the later stages of our model. This is particularly valuable as we may be able to apply MEMRI to resolve the functional loss and recovery of neuronal connectivity [24], as well as brain activation upon drug treatment [25].

To our knowledge, this is the first attempt to apply dynamic MEMRI to examine the extent of glaucomatous involvement and its spread within the entire rat primary visual system *in vivo*. These may help understand the disease mechanisms, monitor the effect of drug interventions to glaucoma models and complement the conventional histological and electrophysiological techniques in examining the glaucomatous visual components.

II. MATERIALS AND METHODS

A. Animal Preparation

Sprague-Dawley female rats (250-280g, 3 months old, N=20) were divided into 3 groups and were prepared to induce ocular hypertension unilaterally in the right eye by photocoagulation of episcleral and limbal veins using an argon laser [13] except in the Control group (Fig. 1). A second laser treatment in the same settings was applied 7 days later to maintain a consistent IOP elevation by about 1.6 times above the normal level. The rats were scanned 2 weeks (n=6), 4 weeks (n =6) and 6 weeks (n =6) after 1st laser treatment. MEMRI was performed 2 to 5 hours (all groups except Week 4), and 8 and 24 hours (Week 4 & Control) after Mn^{2+} injection.

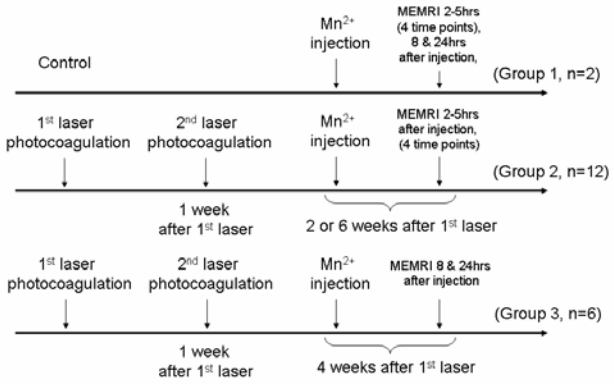

Fig.1. Schedule of 1st and 2nd laser treatments, Mn^{2+} injection and MEMRI scans.

$MnCl_2$ solution (50mM, 3μL) was injected intravitreally into both eyes of the rats after they were anaesthetized with an intraperitoneal injection of a mixture of ketamine (70mg/kg) and xylazine (7mg/kg). The rats were then returned to the cage, and laid prone under a warm lamp until their recovery. Throughout the experiments, the left eye served as a control.

B. MRI protocols

All MRI measurements were acquired on a PharmaScan 70/16 7 T scanner (Bruker, Germany) using a 38mm rat brain quadrature resonator for RF measurement and receiving. Under inhaled isoflurane anaesthesia (2% induction and 1% maintenance), animals were kept warm on a heating pad circulated with water at 37°C and were imaged using an isotropic T1-weighted 3D RARE sequence with TR/TE = 300/6.6ms, flip angle = 180°, RARE factor = 4, FOV = 3.24cm x 3.24cm x 2.47cm and voxel resolution = 193μm x 193μm x 193μm. 2 averages were used and the total acquisition time was 39.5 minutes for each image set. At 2 to 5 hours after Mn^{2+} injection, 4 image sets were obtained for Groups 1 and 2 and a dynamic profile was produced.

C. Data Analysis

All 3D images were co-registered using AIR v5.2.5 (Roger Woods, UCLA) and were analyzed using ImageJ v1.37 (Wayne Rasband, NIH, USA) and BrainSuite v2.0 (LONI, UCLA). Regions of interest (ROIs) were drawn manually on both sides of the vitreous humor, retina, prechiasmatic ON, LGN, SC and the visual cortex at Bregma -5.28mm [26], and the ROIs were copied for each sample. Each value was normalized to the phantom containing 0.05mM of $MnCl_2$ solution in the same slice. Differences between mean values of the ROIs of both sides were compared using two-tail paired t-tests, and the mean values among animal groups or along the time course were compared using ANOVA. Results were considered to be significantly different when $p<.05$.

III. RESULTS

A. Time Profile in Vitreous Humor

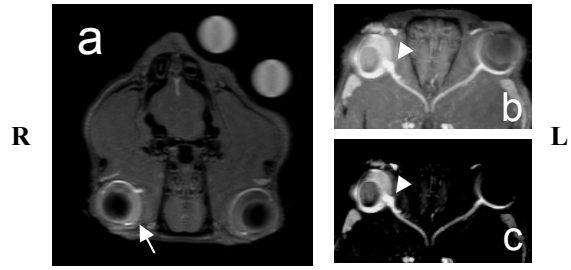

Fig.2. (a) Typical T1W image showing the higher signal intensity in the vitreous humor of the glaucomatous eye (arrow) 6 weeks after 1st laser treatment. (b,c) Maximum intensity projected images on the eyeballs and optic nerves of the same rat (b) before and (c) after windowing.

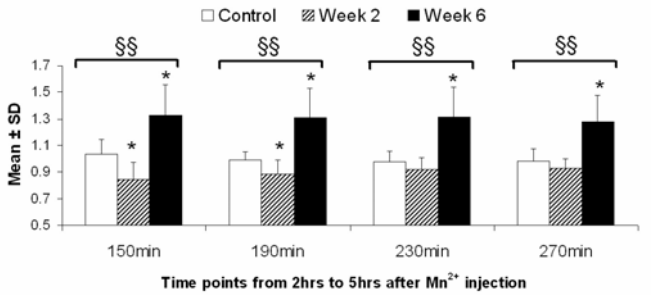

Fig. 3. Ratios of signal intensities in the vitreous humor between the glaucomatous and the contralateral eyes. (two-tail paired t-tests between right and left eyes, *p<.05; ANOVA among animal groups, §§p<.01)

Signal intensities (SI) in the vitreous humor of both eyes decreased as time progressed for all groups (data not shown). The vitreous humor in the glaucomatous eye had a higher signal intensity than the contralateral side in Week animals but not in the Week 2 or the Control groups (Figs. 2 & 3).

B. The Retina and the Optic Nerve Head

There was no statistically significant difference in total retinal thickness between the glaucomatous and the control eyes of the same animal in the Week 6 model (p=0.09). Nevertheless, there was an apparent accumulation of Mn^{2+} ions in the ONHs, more being in the glaucomatous eye in 8 out of the 12 animals examined in Group 2 (arrowheads, Figs. 2b & 2c).

C. The Prechiasmatic Optic Nerve

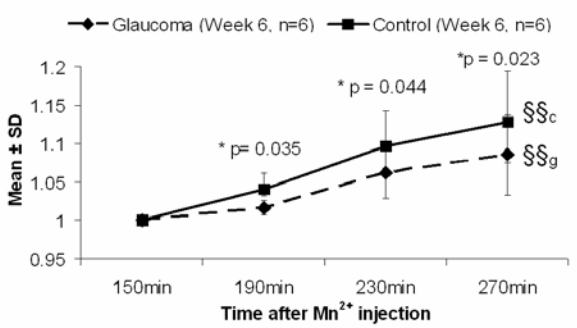

Fig. 4. SI profile of prechiasmatic ON normalized to the first time point in the Week 6 model (two-tail paired t-tests between left and right ON, *p<.05; ANOVA across timeline, §§p<.01).

An apparent reduction in the rate of Mn^{2+} transport was observed at the prechiasmatic region of the glaucomatous ON compared to the contralateral side in the Week 6 model with its significance as shown in Fig. 4.

D. Distal Components of the Rat Visual Pathway

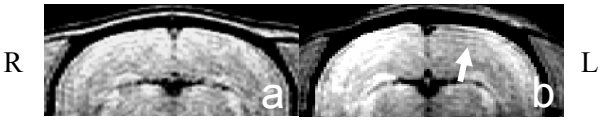

Fig. 5. Windowed T1W images of the visual cortex in (a) Week 2 and (b) Week 6 groups 5 hours after Mn^{2+} injection. Arrow indicates a reduced signal enhancement as compared to the contralateral side of the visual cortex.

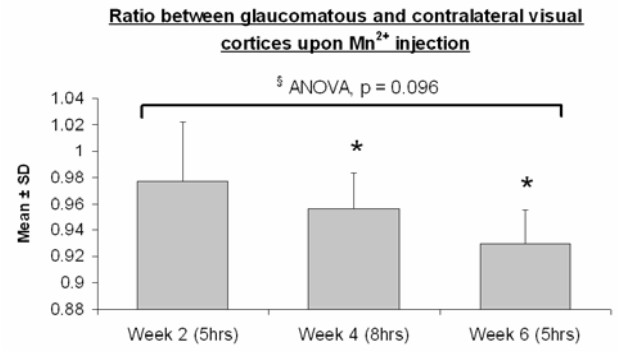

Fig. 6. Ratios between signal intensities of the glaucomatous and the contralateral sides of the visual cortex in different groups. Brackets indicate time after Mn^{2+} injection. (two-tail paired t-tests between left and right visual cortex, *p<.05)

The left visual cortex projected from the glaucomatous eye showed a significant reduction in signal enhancement in the Week 4 and Week 6 models compared to the contralateral side (Figs. 5 & 6). Meanwhile, there was a trend of reducing ratios from Week 2 to Week 6 after 1st laser treatment (Fig.6, ANOVA: p=0.096), indicating a potential, continual decrease of signal enhancement in the left visual cortex; Neither LGN nor SC showed significant differences in the Week 4 model 8 or 24 hours after Mn^{2+} injection (p>.05).

IV. DISCUSSION

A. Accumulation of Mn^{2+} in the Vitreous Humor

Previous studies in normal eyes reported that intravitreal injection of similar dosages of Mn^{2+} reached the retinal boundary at 35 minutes after intravitreal injection, with no diffusion into the lens within the first 53 minutes [11]. The reduction in signal intensities in our experiments from 2 to 5 hours might therefore indicate the continual clearance of Mn^{2+} away from the posterior chamber via aqueous outflow or by entering the RGCs via Ca^{2+} channels upon depolarization [7].

The higher signal intensity observed in the vitreous humor in the glaucomatous eye might result from the blockade of the conventional trabecular route drained by the episcleral veins upon photocoagulation. Meanwhile, previous findings showed an RGC loss of 13%, 22% and 25% at 2, 4 and 8 weeks respectively after laser treatment in identical models [13]. Together with the possible occlusion in the ONH [1], these might also reduce the neuronal uptake of Mn^{2+} ions into the intracellular space, causing an accumulation in the vitreous humor. There was a slight decrease in the ratio for the Week 2 model compared to the Control group in Fig. 3, potentially due to the increased convective flow upon IOP rise in the glaucomatous eye while the RGC loss was little [27]. It is apparent that the usual pattern of Mn^{2+} clearance in the glaucomatous eyeball was perturbed upon intravitreal injection.

B. Total Retinal Thickness and Optic Nerve Head Occlusion

The retinal structure was shown to remain intact in animals with mild-to-moderate IOP elevation [13]. Despite the possible discrepancies from partial volume effect, the insignificant change in total retinal thickness in our model correlated with previous histological findings in identical models 8 weeks after 1st laser treatment [13].

The Mn^{2+} accumulation in the ONH might be due to uptake by glia and connective tissue cells via extra-axonal diffusion [9, 28] since the rat lamina cribrosa is relatively sparse [4]; Meanwhile, the apparent accumulation of Mn^{2+} ions being more in the glaucomatous ONH might suggest the swelling of axons with a deposition of membranous organelles, whose fast axonal movement was expected to be disturbed at the pores of the connective tissues in the lamina cribrosa [29].

C. Mn^{2+} Transport along the Optic Nerve

There was an apparent reduction in the rate of Mn^{2+} transport in the prechiasmatic ON in the glaucomatous eye in the Week

6 model (Fig. 4). This might be suggestive of an obstruction in axoplasmic transport along the ON, a reduction in the axonal densities in the glaucomatous ONs and/or a reduction in Mn^{2+} uptake into the RGCs due to the RGC loss. Further investigations should increase the resolution of MRI acquisitions and the number of time points so as to better delineate the SI profile along the entire rat ON and to draw more confirmative conclusions.

D. Reduced Signal Enhancements in Visual Cortex

In the albino rats, more than 98.5% of the RGC axons decussate to the contralateral side of the visual pathway at the optic chiasm [30]. The prominent reduction in SI in the left visual cortex, whose fibers were projected mainly from the glaucomatous eye transsynaptically via LGN and SC, was found at 5.28mm posterior to bregma in the later stages of our disease model (Figs. 5 & 6). This might suggest a delayed arrival of Mn^{2+} ions in the visual cortex detectable by MRI via fast axonal transport; Apart from fast axonal transport, another possible explanation might arise from the decrease in activated regions in the visual cortex due to visual field deficits or degenerative changes in the cortex [22]. Mn^{2+} might be released to the systemic circulation after absorption by the capillary vessels in the retina [31], and be uptaken by the active cells in the visual cortex [21] to a detectable amount upon windowing [5]. A decrease in the amount of active cells would certainly increase the difficulty to detect the enhanced regions of the visual cortex by MEMRI.

In recent human studies, occipital proton magnetic resonance spectroscopy (^{1}H-MRS) revealed insignificant changes in metabolite concentrations upon progressive retinal visual field defects [32], possibly due to the metabolite change being too slow to be detectable. Nevertheless, functional MRI has successfully demonstrated the relationship of the functional organization of primary visual cortex (V1) with the damage to the optic disc and the visual field loss in primary open-angle glaucoma (POAG) [33-34]. By applying MEMRI, we provided a global view of the extent of glaucomatous involvement and its spread within the rat primary visual system *in vivo*. This may complement other histological and MRI techniques to define the defective location specifically and conveniently for finer research, and may help monitor the effect of drug interventions, e.g. the neuroprotective effect of Lycium barbarum Lynn [35] to the glaucoma models globally and longitudinally. Limitations in this experiment include technical errors in surgical procedures.

V. CONCLUSION

MEMRI potentially provides an *in vivo*, longitudinal and three-dimensional means to investigate the abnormalities in the primary visual system in the rat model of chronic glaucoma.

ACKNOWLEDGMENT

This work was in part supported by Hong Kong Research Grant Council and The University of Hong Kong CRCG.

REFERENCES

[1] S. Thanos and R. Naskar, "Correlation between retinal ganglion cell death and chronically developing inherited glaucoma in a new rat mutant," Exp Eye Res, vol. 79, pp. 119-29, Jul 2004.
[2] H. A. Quigley and A. T. Broman, "The number of people with glaucoma worldwide in 2010 and 2020," Br J Ophthalmol, vol. 90, pp. 262-7, Mar 2006.
[3] P. L. Kaufman, "Nitric-oxide synthase and neurodegeneration/neuroprotection," Proc Natl Acad Sci U S A, vol. 96, pp. 9455-6, Aug 17 1999.
[4] J. C. Morrison, "Elevated intraocular pressure and optic nerve injury models in the rat," J Glaucoma, vol. 14, pp. 315-7, Aug 2005.
[5] J. D. Lindsey, M. Scadeng, D. J. Dubowitz, J. G. Crowston, and R. N. Weinreb, "Magnetic resonance imaging of the visual system in vivo: transsynaptic illumination of V1 and V2 visual cortex," Neuroimage, vol. 34, pp. 1619-26, Feb 15 2007.
[6] A. C. Silva, J. H. Lee, I. Aoki, and A. P. Koretsky, "Manganese-enhanced magnetic resonance imaging (MEMRI): methodological and practical considerations," NMR Biomed, vol. 17, pp. 532-43, Dec 2004.
[7] R. G. Pautler, "Biological applications of manganese-enhanced magnetic resonance imaging," Methods Mol Med, vol. 124, pp. 365-86, 2006.
[8] R. G. Pautler, "In vivo, trans-synaptic tract-tracing utilizing manganese-enhanced magnetic resonance imaging (MEMRI)," NMR Biomed, vol. 17, pp. 595-601, Dec 2004.
[9] T. Watanabe, J. Frahm, and T. Michaelis, "Functional mapping of neural pathways in rodent brain in vivo using manganese-enhanced three-dimensional magnetic resonance imaging," NMR Biomed, vol. 17, pp. 554-68, Dec 2004.
[10] S. A. Molokhia, E. K. Jeong, W. I. Higuchi, and S. K. Li, "Examination of penetration routes and distribution of ionic permeants during and after transscleral iontophoresis with magnetic resonance imaging," Int J Pharm, vol. 335, pp. 46-53, Apr 20 2007.
[11] S. K. Li, E. K. Jeong, and M. S. Hastings, "Magnetic resonance imaging study of current and ion delivery into the eye during transscleral and transcorneal iontophoresis," Invest Ophthalmol Vis Sci, vol. 45, pp. 1224-31, Apr 2004.
[12] J. C. Morrison, F. W. Fraunfelder, S. T. Milne, and C. G. Moore, "Limbal microvasculature of the rat eye," Invest Ophthalmol Vis Sci, vol. 36, pp. 751-6, Mar 1995.
[13] R. S. Li, D. K. Tay, H. H. Chan, and K. F. So, "Changes of retinal functions following the induction of ocular hypertension in rats using argon laser photocoagulation," Clin Experiment Ophthalmol, vol. 34, pp. 575-83, Aug 2006.
[14] B. A. Berkowitz, R. Roberts, D. J. Goebel, and H. Luan, "Noninvasive and simultaneous imaging of layer-specific retinal functional adaptation by manganese-enhanced MRI," Invest Ophthalmol Vis Sci, vol. 47, pp. 2668-74, Jun 2006.
[15] R. D. Braun, M. Gradianu, K. S. Vistisen, R. L. Roberts, and B. A. Berkowitz, "Manganese-enhanced MRI of human choroidal melanoma xenografts," Invest Ophthalmol Vis Sci, vol. 48, pp. 963-7, Mar 2007.
[16] K. D. Smith, V. Kallhoff, H. Zheng, and R. G. Pautler, "In vivo axonal transport rates decrease in a mouse model of Alzheimer's disease," Neuroimage, Feb 12 2007.
[17] S. Ryu, S. L. Brown, A. Kolozsvary, J. R. Ewing, and J. H. Kim, "Noninvasive detection of radiation-induced optic neuropathy by manganese-enhanced MRI," Radiat Res, vol. 157, pp. 500-5, May 2002.
[18] M. Thuen, T. E. Singstad, T. B. Pedersen, O. Haraldseth, M. Berry, A. Sandvig, and C. Brekken, "Manganese-enhanced MRI of the optic visual pathway and optic nerve injury in adult rats," J Magn Reson Imaging, vol. 22, pp. 492-500, Oct 2005.
[19] D. Banerjee, B. Hegedus, D. H. Gutmann, and J. R. Garbow, "Detection and measurement of neurofibromatosis-1 mouse optic glioma in vivo," Neuroimage, Feb 23 2007.
[20] P. K. Khosla, S. Patra, P. Prakash, and K. S. Ratnakar, "Axoplasmic transport in optic nerve (an experimental study in rabbits)," Indian J Ophthalmol, vol. 30, pp. 23-8, Jan 1982.
[21] I. Aoki, Y. J. Wu, A. C. Silva, R. M. Lynch, and A. P. Koretsky, "In vivo detection of neuroarchitecture in the rodent brain using manganese-enhanced MRI," Neuroimage, vol. 22, pp. 1046-59, Jul 2004.
[22] N. Gupta and Y. H. Yucel, "Glaucoma as a neurodegenerative disease," Curr Opin Ophthalmol, vol. 18, pp. 110-4, Mar 2007.
[23] N. Gupta, L. C. Ang, L. Noel de Tilly, L. Bidaisee, and Y. H. Yucel, "Human glaucoma and neural degeneration in intracranial optic nerve, lateral geniculate nucleus, and visual cortex," Br J Ophthalmol, vol. 90, pp. 674-8, Jun 2006.
[24] J. P. van der Zijden, O. Wu, A. van der Toorn, T. P. Roeling, R. L. Bleys, and R. M. Dijkhuizen, "Changes in neuronal connectivity after stroke in rats as studied by serial manganese-enhanced MRI," Neuroimage, vol. 34, pp. 1650-7, Feb 15 2007.
[25] H. Lu, Z. X. Xi, L. Gitajn, W. Rea, Y. Yang, and E. A. Stein, "Cocaine-induced brain activation detected by dynamic manganese-enhanced magnetic resonance imaging (MEMRI)," Proc Natl Acad Sci U S A, vol. 104, pp. 2489-94, Feb 13 2007.
[26] G. Paxinos, C. Watson, "The Rat Brain in Stereotaxic Coordinates," Academic Press, San Diego, 2005.
[27] J. Xu, J. J. Heys, V. H. Barocas, and T. W. Randolph, "Permeability and diffusion in vitreous humor: implications for drug delivery," Pharm Res, vol. 17, pp. 664-9, Jun 2000.
[28] A. C. Taylor and P. Weiss, "Demonstration of axonal flow by the movement of tritium-labeled protein in mature optic nerve fibers," Proc Natl Acad Sci U S A, vol. 54, pp. 1521-7, Dec 1965.
[29] M. E. Pease, S. J. McKinnon, H. A. Quigley, L. A. Kerrigan-Baumrind, and D. J. Zack, "Obstructed axonal transport of BDNF and its receptor TrkB in experimental glaucoma," Invest Ophthalmol Vis Sci, vol. 41, pp. 764-74, Mar 2000.
[30] M. D. Fleming, R. M. Benca, and M. Behan, "Retinal projections to the subcortical visual system in congenic albino and pigmented rats," Neuroscience, vol. 143, pp. 895-904, Dec 2006.
[31] T. Watanabe, T. Michaelis, and J. Frahm, "Mapping of retinal projections in the living rat using high-resolution 3D gradient-echo MRI with Mn2+-induced contrast," Magn Reson Med, vol. 46, pp. 424-9, Sep 2001.
[32] C. C. Boucard, J. M. Hoogduin, J. van der Grond, and F. W. Cornelissen, "Occipital Proton Magnetic Resonance Spectroscopy (H-MRS) Reveals Normal Metabolite Concentrations in Retinal Visual Field Defects," PLoS ONE, vol. 2, p. e222, 2007.
[33] R. O. Duncan, P. A. Sample, R. N. Weinreb, C. Bowd, and L. M. Zangwill, "Retinotopic organization of primary visual cortex in glaucoma: a method for comparing cortical function with damage to the optic disk," Invest Ophthalmol Vis Sci, vol. 48, pp. 733-44, Feb 2007.
[34] R. O. Duncan, P. A. Sample, R. N. Weinreb, C. Bowd, and L. M. Zangwill, "Retinotopic organization of primary visual cortex in glaucoma: Comparing fMRI measurements of cortical function with visual field loss," Prog Retin Eye Res, vol. 26, pp. 38-56, Jan 2007.
[35] H. C. Chan, R. C. Chang, A. Koon-Ching Ip, K. Chiu, W. H. Yuen, S. Y. Zee, and K. F. So, "Neuroprotective effects of Lycium barbarum Lynn on protecting retinal ganglion cells in an ocular hypertension model of glaucoma," Exp Neurol, vol. 203, pp. 269-73, Jan 2007.